

Non-linearity and non-smoothness in multi-body dynamics: application to woodpecker toy

J Slavič and M Boltežar*

Laboratory for Dynamics of Machines and Structures, University of Ljubljana, Ljubljana, Slovenia

The manuscript was received on 16 June 2004 and was accepted after revision for publication on 19 April 2005.

DOI: 10.1243/095440605X31562

Abstract: The introduction of the article gives a short historical overview of the modelling of multi-body dynamics with unilateral contacts. The unilateral contacts formulation as introduced by Pfeiffer and Glocker is adapted to discretely defined body shapes. By using two-step collision detection, a fast and exact collision detection is achieved. The procedures are tested on a numerical example of the woodpecker toy and the results are compared with those of other authors who used a simpler mathematical model.

Keywords: rigid multi-body dynamics, unilateral contacts, discrete, collision detection, friction, woodpecker

1 INTRODUCTION

The mathematical formulation of multi-body dynamics with unilateral contacts received much interest in recent decades; however, it was only in the last decade that the formulation has been developed to the necessary mathematical and physical consistency. Some of the first studies on multi-body dynamics with a bilateral contact were done by Vereshchagin [1], Armstrong and Green [2], and Featherston [3] in the 1970s and 1980s. The first studies of unilateral contacts as a linear complementarity problem (LCP) were published by Lötstedt [4, 5]. Lötstedt was used as a basis by several other researchers such as Murty [6], Baraff [7], Panagiotopoulos [8], Moreau [9], and Mirtich and Canny [10].

In recent years, the *time-stepping methods* have developed particularly rapidly [11, 12]. These methods operate in the impulse–velocity domain; therefore, at impact there is no need to switch from the force–acceleration domain to the impulse–velocity domain, which allows longer time-steps and avoids problems with the existence of a solution at high friction. An important contribution to the time-stepping methods was made by Monteiro-Marques [13], who studied the convergence of the

solution and also by Stewart and Trinkle [14, 15], Anitescu and Potra [16], and others.

Because the time-stepping methods lack precision, we decided to use the formulation of Pfeiffer and Glocker [17]; their work presents a mathematically clear and physically consistent basis for plane contact dynamics and is superior to the classical approach in its uniform way of solving the stick–slip, detachment and impact events. There is also no need to adopt a number of generalized coordinates at any time. The strength of the formulation is in its simplicity and generality of use. Pfeiffer and Glocker introduced a new friction decomposition that avoids singularities in the presence of dependent coordinates and can also handle over-constrained systems. They introduced, for the first time, the impact law with friction as an LCP.

The aim of this paper is to adapt the formulation [18, 17] of multi-body plane dynamics with unilateral contacts to discretely defined bodies with arbitrary body shapes. The procedures will be presented using the example of the woodpecker toy, which has already been extensively studied by other researchers.

The organization of the paper is as follows. In section 2, the basics of multi-body dynamics with unilateral contacts are presented. Section 3 discusses the changes needed for discrete bodies simulations and presents a fast but exact two-step collision detection. In section 4, a numerical example with the implementation of the mathematical formulation is discussed. Section 5 presents the conclusions.

*Corresponding author: Laboratory for Dynamics of Machines and Structures, Faculty of Mechanical Engineering, University of Ljubljana, Ljubljana, Slovenia

2 MULTI-BODY DYNAMICS WITH UNILATERAL CONTACTS AS AN LCP

For the sake of completeness, this section gives a brief review of the mathematical modelling of multi-body dynamics with unilateral contacts as presented by Pfeiffer and Glocker [17, 18]. The methods are presented for linear contacts (plain dynamics), but with some modifications they can also be used for plane contacts.

The equations of motion for a multi-body system with f degrees of freedom (including bilateral contacts) can be written as

$$\mathbf{M}(\mathbf{q}, t)\ddot{\mathbf{q}} - \mathbf{h}(\mathbf{q}, \dot{\mathbf{q}}, t) = \mathbf{0} \in \mathbb{R}^f \tag{1}$$

where \mathbf{M} is the mass matrix, \mathbf{q} is the vector of generalized coordinates, and \mathbf{h} is the vector of generalized active forces. If there is a set of $i \in I_N$ contact forces then the equations of motion will be

$$\mathbf{M}\ddot{\mathbf{q}} - \mathbf{h} = \sum_{i \in I_N} \mathbf{Q}_i^C \in \mathbb{R}^f \tag{2}$$

where \mathbf{Q}_i^C are the generalized, non-conservative active forces.

Note that the contact forces change the number of degrees of freedom. In general, it is not known which degrees of freedom disappear; this problem is usually solved by looking at all the possible solutions and finding the one that is physically consistent. If there are n_N possible contact points with a stick–slip transition or detachment, then there are 3^{n_N} possible solutions [17]. It is clear that the search for a physically consistent combination is time-consuming. In addition, for numerical simulations, it is quite unsuitable to change the number of the minimum number of coordinates during each time-step.

As discussed subsequently, the LCP method solves this problem in an elegant way, and the number of generalized coordinates is constant at all times. The number of generalized coordinates is always equal to the number of degrees of freedom of the system without unilateral contacts (2).

The real contact forces are linked with the generalized contact forces via the Jacobian matrix. In Fig. 1, bodies are shown, the centres of gravity being denoted by A and B. The normal contact force $\mathbf{F}_{A,N}$ at point C_A on the body A as a generalized contact force is

$$\mathbf{Q}_{A,N}^C = \left(\frac{\partial \mathbf{r}_{C_A}}{\partial \mathbf{q}} \right)^T \mathbf{F}_{A,N} = \mathbf{J}_{C_A}^T \cdot \mathbf{n}_A \cdot \lambda_N \tag{3}$$

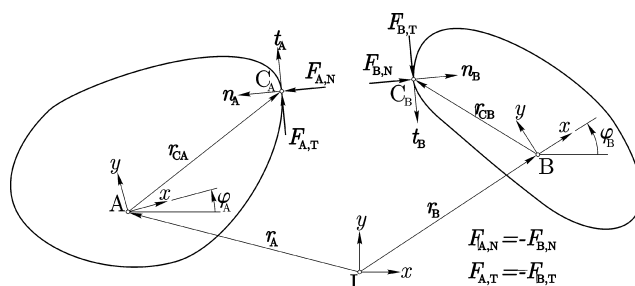


Fig. 1 Contact forces

where $\mathbf{J}_{C_A}^T$ is the Jacobian matrix of ${}^I\mathbf{r}_{C_A}$ and when including the normal force at point B, then \mathbf{Q}_N^C becomes

$$\mathbf{Q}_N^C = (\mathbf{J}_{C_A}^T \mathbf{n}_A + \mathbf{J}_{C_B}^T \mathbf{n}_B) \lambda_N = \boldsymbol{\omega}_N \lambda_N \tag{4}$$

$\boldsymbol{\omega}_N$ includes the kinematical properties of the contact, λ_N is the amplitude of the force, and I denotes the inertial frame.

By using a similar notation for the tangential force (index T), equation (2) is rewritten as

$$\mathbf{M}\ddot{\mathbf{q}} - \mathbf{h} - \sum_{i \in I_N} (\mathbf{w}_N \lambda_N + \mathbf{w}_T \lambda_T)_i = \mathbf{0} \in \mathbb{R}^f \tag{5}$$

or by using matrix notation

$$\mathbf{W}_N = \{\mathbf{w}_{Ni}\}, \quad \mathbf{W}_T = \{\mathbf{w}_{Ti}\}, \quad i \in I_N \tag{6}$$

the equations of motion are

$$\mathbf{M}\ddot{\mathbf{q}} - \mathbf{h} - (\mathbf{W}_N \mathbf{W}_T) \begin{pmatrix} \lambda_N \\ \lambda_T \end{pmatrix} = \mathbf{0} \in \mathbb{R}^f \tag{7}$$

The contact situations are solved in two steps: in the first, the non-smooth impact with friction is solved and in the second, the stick–slip or detachment situation is solved. The impact is solved and in the impulse-domain, whereas the stick–slip or detachment is solved in the force-domain.

All the possible contact points I_G are organized in four sets during each time-step

$$\begin{aligned} I_G &= \{1, 2, \dots, n_G\} \\ I_S &= \{i \in I_G; \dot{g}_N = 0\} & n_S \text{ elements} \\ I_N &= \{i \in I_S; \dot{g}_N < 0\} & n_N \text{ elements} \\ I_H &= \{i \in I_N; \dot{g}_T = 0\} & n_H \text{ elements} \end{aligned} \tag{8}$$

The set I_S contains all the closed contacts, the set I_N contains only the contacts with vanishing relative normal velocities (stick–slip or detachment), and the set I_H contains the possibly sticking contacts.

The number of elements in the sets can change during each time-step.

2.1 Stick-slip transition or detachment

First, the stick-slip transition or detachment problem is solved on an impact-free set I_N . The equations of motion (7) and the relative contact accelerations $\ddot{\mathbf{g}}$ are [17–19]

$$M\ddot{\mathbf{q}} - \mathbf{h} - (\mathbf{W}_N + \mathbf{W}_G \bar{\boldsymbol{\mu}}_G \mathbf{W}_H) \begin{pmatrix} \boldsymbol{\lambda}_N \\ \boldsymbol{\lambda}_H \end{pmatrix} = \mathbf{0} \in \mathbb{R}^f \quad (9)$$

$$\begin{pmatrix} \ddot{\mathbf{g}}_N \\ \ddot{\mathbf{g}}_H \end{pmatrix} = \begin{pmatrix} \mathbf{W}_N^T \\ \mathbf{W}_H^T \end{pmatrix} \ddot{\mathbf{q}} + \begin{pmatrix} \bar{\mathbf{w}}_N \\ \bar{\mathbf{w}}_H \end{pmatrix} \in \mathbb{R}^{n_N+n_H} \quad (10)$$

The index N denotes the normal direction and the index H denotes the tangential direction of the possibly sticking set I_H . The new index G denotes the sliding contacts (the tangential force is known) of the set $I_N \setminus I_H$ and the $\bar{\boldsymbol{\mu}}_G$ diagonal matrix of friction coefficients.

Each closed contact $i \in I_N$ is characterized by a vanishing contact distance $g_{Ni} = 0$ and a normal relative velocity $\dot{g}_{Ni} = 0$. Because of the impenetrability of the bodies $g_{Ni} \geq 0$, a complementary solution for each contact in the normal direction can be found

$$\ddot{g}_{Ni} = 0 \wedge \lambda_{Ni} \geq 0 \quad \text{contact is maintained} \quad (11)$$

$$\ddot{g}_{Ni} > 0 \wedge \lambda_{Ni} = 0 \quad \text{detachment} \quad (12)$$

It is clear that the product of the contact force and the relative acceleration is zero for all $i \in I_N$

$$\ddot{g}_{Ni} \lambda_{Ni} = 0 \quad (13)$$

Such a complementarity is sometimes also referred to as the corner law [20] and is shown in Fig. 2. In the following, we will also try to represent the idea of the corner law in the tangential direction. Figure 3(a) presents the Coulomb friction law. Figure 3(b) shows the friction law decomposed into two branches: one for positive sliding and another

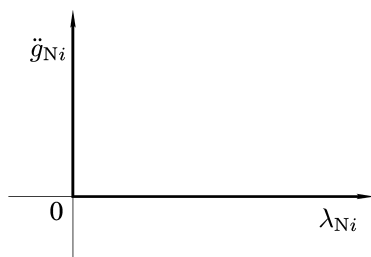


Fig. 2 Complementarity in the normal direction

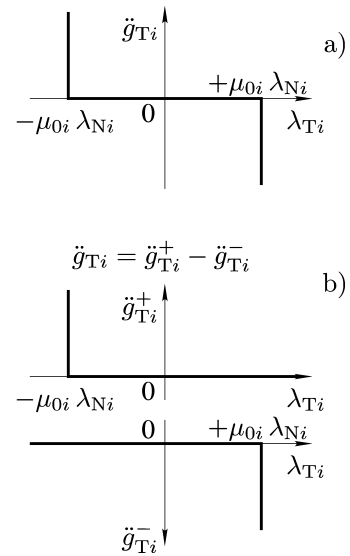


Fig. 3 Complementarity in the tangential direction

for negative sliding. For each branch, a linear complementarity is

$$\ddot{g}_{Ti} = 0 \wedge \lambda_{Ti} + \mu_{0i} \lambda_{Ni} \geq 0 \quad \text{remains sticking} \quad (14)$$

$$\ddot{g}_{Ti} > 0 \wedge \lambda_{Ti} + \mu_{0i} \lambda_{Ni} = 0 \quad \text{positive sliding} \quad (15)$$

and for all $i \in I_N$

$$\ddot{g}_{Ti} (\lambda_{Ti} + \mu_{0i} \lambda_{Ni}) = 0 \quad (16)$$

In a similar manner, an LCP for negative sliding is built. In reality, we used a slightly different decomposition for the tangential direction, as shown in Fig. 3. The decomposition was presented by Pfeiffer and Glocker [17] and avoids singularities in the case of dependent constraints.

By extensive mathematical manipulation [17], the normal and tangential directions are written together in the form

$$\mathbf{y} = \mathbf{A}\mathbf{x} + \mathbf{b} \quad (17)$$

$$\mathbf{y} \geq 0, \quad \mathbf{x} \geq 0, \quad \mathbf{y}^T \mathbf{x} = 0 \quad (18)$$

Equations (17) and (18) represent an LCP where the vectors $\{\mathbf{y}, \mathbf{x}\} \in \mathbb{R}^{n_N+4n_H}$ are not known, but they comply with the complementary conditions (18), where $\mathbf{y}^T \mathbf{x} = 0$ should be understood on the element basis: $y_i x_i = 0$ for all i . Vector \mathbf{y} includes the unknown contact accelerations $\ddot{\mathbf{g}}$ and vector \mathbf{x} includes the unknown contact forces $\boldsymbol{\lambda}$. \mathbf{A} and \mathbf{b} are the known matrix and vector defined by the mass matrix, the friction coefficients, and the contact shapes.

2.1.1 Linear complementarity problem

Equations (17) and (18) represent an LCP [21]. The only known algorithms that guarantee to solve the LCP are the *enumerative methods* [6]. As the enumerative methods take 2^n possible different combinations of $x_i y_i$ (for a matrix \mathbf{A} of dimension n), it is clear that the enumerative methods are appropriate for small values of n only.

A quicker way of solving the LCP is the *complementarity pivot algorithm*, presented by Cottle and Dantzig [21], which is usually referred to as Lemke’s algorithm. Lemke’s algorithm is based on the simplex method and uses a basis vector with an artificial variable z . The process can terminate into two ways: through the iterative process, either z can be dropped out of the basis vector (we found a solution) or z cannot be dropped out. In the second case, the solution might not exist or it cannot be found [22]. However, if the matrix \mathbf{A} is positive-semidefinite, the solution is guaranteed to converge [6]. Lemke’s algorithm includes a matrix inversion during each iteration step. Because only one column is changed during each iteration step, a considerable reduction in computation time can be gained by using the Sherman–Morrison–Woodbury formula [22, 23].

2.2 Impact with friction

The stick–slip or detachment transition is solved in the force–acceleration domain, whereas the impact is solved in the impulse–velocity domain. Some common assumptions for rigid-body impacts are made. The duration of the impact is infinitely short, the wave effects are not taken into account, during the impact all positions and orientations, and all the non-impulsive forces and torques remain constant. The impact is divided into two phases: the compression phase (time interval: $t_A - t_C$) and the expansion phase (time interval: $t_C - t_E$). In this work, Poisson’s impact law is used.

For impacts, the contacts of the set I_S are taken into account.

2.2.1 Compression phase

The index C is used for the compression phase. By integrating the equation of motion (7) an impulse-domain equation is built [17]

$$\mathbf{M}(\dot{\mathbf{q}}_C - \dot{\mathbf{q}}_A) - (\mathbf{W}_N \mathbf{W}_T) \begin{pmatrix} \Lambda_{NC} \\ \Lambda_{TC} \end{pmatrix} = \mathbf{0} \in \mathbb{R}^f \quad (19)$$

The relative contact velocities are

$$\begin{pmatrix} \dot{\mathbf{g}}_{NC} \\ \dot{\mathbf{g}}_{TC} \end{pmatrix} = \begin{pmatrix} \mathbf{W}_N^T \\ \mathbf{W}_T^T \end{pmatrix} (\dot{\mathbf{q}}_C - \dot{\mathbf{q}}_A) + \begin{pmatrix} \dot{\mathbf{g}}_{NA} \\ \dot{\mathbf{g}}_{TA} \end{pmatrix} \in \mathbb{R}^{2n_s} \quad (20)$$

Λ_{NC} and Λ_{TC} are the contact impulses during the compression phase, and A and C represent the beginning and the end of compression. Similarly, as before, complementarity conditions in the normal and tangential directions can be found (Fig. 4).

After decomposing the tangential direction and after expansive mathematical manipulation, an LCP of the form (17) can be stated. Vector $\mathbf{y} \in \mathbb{R}^{5n_s}$ contains the relative contact velocities at the end of the compression and vector $\mathbf{x} \in \mathbb{R}^{5n_s}$ the contact impacts during compression.

2.2.2 Expansion phase

After solving the compression phase, we have to solve the expansion phase (index E)

$$\mathbf{M}(\dot{\mathbf{q}}_E - \dot{\mathbf{q}}_C) - (\mathbf{W}_N \mathbf{W}_T) \begin{pmatrix} \Lambda_{NE} \\ \Lambda_{TE} \end{pmatrix} = \mathbf{0} \in \mathbb{R}^f \quad (21)$$

$$\begin{pmatrix} \dot{\mathbf{g}}_{NE} \\ \dot{\mathbf{g}}_{TE} \end{pmatrix} = \begin{pmatrix} \mathbf{W}_N^T \\ \mathbf{W}_T^T \end{pmatrix} (\dot{\mathbf{q}}_E - \dot{\mathbf{q}}_C) + \begin{pmatrix} \dot{\mathbf{g}}_{NC} \\ \dot{\mathbf{g}}_{TC} \end{pmatrix} \in \mathbb{R}^{2n_s} \quad (22)$$

The complementarity of the expansion phase is shown in Fig. 5. The expansion impulse is proportional to the compression impulse. However, if numerous impacts can occur simultaneously then an impulse at one contact point could result in penetration at some other contact point. As shown in Fig. 5, this is avoided by the complementarity in the normal direction. If the expansion impulse is larger than $\epsilon_{N_i} \Lambda_{NC_i}$ to avoid penetration, then the contact point cannot detach. Using such a notation, the impact law might not be dissipative; however, as shown in reference [17], this is not the case. The LCP impact law of Pfeiffer and Glocker is one of the few which also includes reversibility in the tangential direction (super-elastic balls have this capability). For this reversibility, a new parameter ν , which

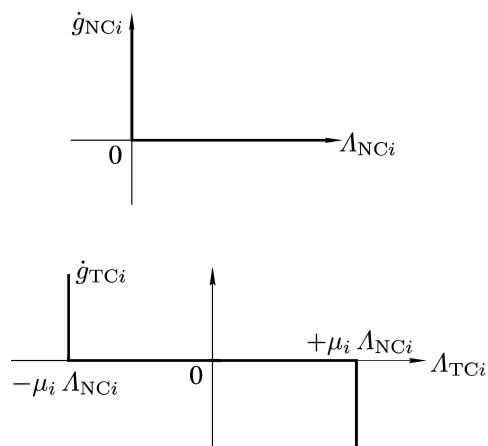


Fig. 4 Complementarity of compression in the normal and tangential directions

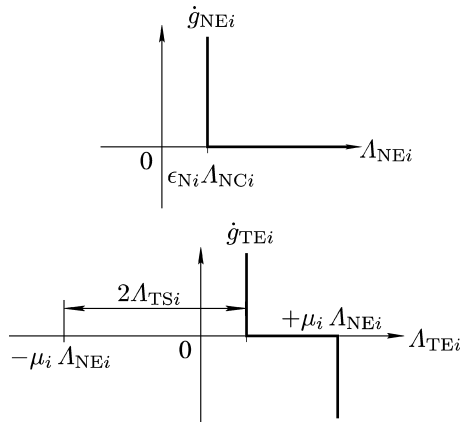


Fig. 5 Complementarity of expansion in the normal and tangential directions

defines the impulse $\Lambda_{TS,i}$, needs to be introduced [17]. As for compression, after extensive mathematical manipulation an LCP of the form (17) can be stated. Vector $\mathbf{y} \in \mathbb{R}^{5n_s}$ contains the relative contact velocities at the end of the expansion phase, whereas the vector $\mathbf{x} \in \mathbb{R}^{5n_s}$ contains the contact impacts of the expansion.

3 INTRODUCTION TO DISCRETE BODIES

The multi-body dynamics as presented earlier is very suitable for completely analytical solving: all one needs to define is the mass matrix \mathbf{M} , the generalized forces \mathbf{h} vector (7), the vector of generalized coordinates \mathbf{q} , and the matrices \mathbf{W}_N and \mathbf{W}_T for all the possible contact points $i \in I_G$. The actual dimension of \mathbf{W}_N and \mathbf{W}_T changes in accordance with the current number of contacts.

The equations of motion for the contact-free case are integrated (i.e. by Runge–Kutta method) until there is at least one closed contact. If there are impacts, then first the compression and expansion phases need to be solved and afterwards the stick–slip or detachment phase also need to be solved. If there is no impact then only the stick–slip or detachment has to be solved.

If the bodies of the system are defined as a discrete polygon (Fig. 6) then the definition of the kinematical parameters \mathbf{W}_N and \mathbf{W}_T of the possible contact points needs to be redefined during each time-step.

3.1 Kinematical parameters of contact points

In this section, we show how to find the matrices \mathbf{W}_N and \mathbf{W}_T for a contact point of two discretely defined bodies. The points of the polygon are defined counter-clockwise relative to the center of gravity. The center of gravity of body A is denoted by A (Figs 1 and 6).

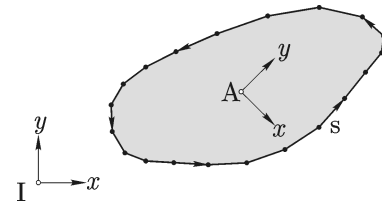


Fig. 6 Discrete polygon

The aim is to find a notation of the contact point of body A by using the Jacobian matrix \mathbf{J}_{C_A} and a vector with acceleration non-dependent values $\bar{\mathbf{j}}_{C_A}$

$${}^I\ddot{\mathbf{r}}_{C_A} = \mathbf{J}_{C_A}\ddot{\mathbf{q}} + \bar{\mathbf{j}}_{C_A} \tag{23}$$

The Jacobian of the contact point of body A is

$$\mathbf{J}_{C_A} = \frac{\partial {}^I\ddot{\mathbf{r}}_{C_A}}{\partial \ddot{\mathbf{q}}} \in \mathbb{R}^{2 \times f} \tag{24}$$

where

$${}^I\ddot{\mathbf{r}}_{C_A} = \ddot{\mathbf{r}}_A + \frac{d^2}{dt^2}(\mathbf{A}_{IA} \mathbf{r}_{CA}) \tag{25}$$

\mathbf{A}_{IA} is a transformation matrix from the relative frame A to the inertial frame I.

The Jacobian of the center of gravity for plane motion is

$$\mathbf{J}_A = \frac{\partial \ddot{\mathbf{r}}_A}{\partial \ddot{\mathbf{q}}} \in \mathbb{R}^{2 \times f} \tag{26}$$

If all the coordinates of ${}^I\ddot{\mathbf{r}}_A$ are in the set of generalized coordinates, then the Jacobian is quite simple. However, in general, this is not the case.

To define the Jacobian of ${}^I\ddot{\mathbf{r}}_{C_A}$, the rotation φ_A around the center of gravity needs to be considered. If the rotation φ_A is in the set of generalized coordinates \mathbf{q} then the Jacobian – because of rotation – is

$$\mathbf{J}_{RA} = \begin{pmatrix} 0 & \cdots & 0 & -y_{CA} \cos \varphi_A & 0 & \cdots & 0 \\ & & & -x_{CA} \sin \varphi_A & & & \\ 0 & \cdots & 0 & +x_{CA} \cos \varphi_A & 0 & \cdots & 0 \\ & & & -y_{CA} \sin \varphi_A & & & \\ \hline & & j-1 & j & j+1 & & \end{pmatrix} \tag{27}$$

where j is the position of φ_A in the vector of generalized coordinates \mathbf{q} and

$${}^A\mathbf{r}_{CA} = \begin{pmatrix} x_{CA} \\ y_{CA} \end{pmatrix} \tag{28}$$

The Jacobian \mathbf{J}_{C_A} and the corresponding vector $\bar{\mathbf{j}}_{C_A}$ are

$$\mathbf{J}_{C_A} = \mathbf{J}_A + \mathbf{J}_{RA} \quad \bar{\mathbf{j}}_{C_A} = \bar{\mathbf{j}}_A + \bar{\mathbf{j}}_{RA} \tag{29}$$

If φ_A is absolute and also a generalized coordinate then

$$\bar{\mathbf{J}}_{RA} = \begin{pmatrix} (-x \cos \varphi_A + y \sin \varphi_A) \dot{\varphi}_A^2 \\ -(y \cos \varphi_A + x \sin \varphi_A) \dot{\varphi}_A^2 \end{pmatrix} \quad (30)$$

In a similar manner, we define the kinematics of the contact point C of the body B (Fig. 1) and finally come to the following vectors \mathbf{w} and scalars \bar{w}

$$\begin{aligned} \mathbf{w}_{N,A} &= \mathbf{J}_{CA}^T \cdot \mathbf{1}n_A + \mathbf{J}_{CB}^T \cdot \mathbf{1}n_B \\ \mathbf{w}_{T,A} &= \mathbf{J}_{CA}^T \cdot \mathbf{1}t_A + \mathbf{J}_{CB}^T \cdot \mathbf{1}t_B \end{aligned} \quad (31)$$

$$\begin{aligned} \bar{w}_{N,A} &= \bar{\mathbf{J}}_{CA}^T \cdot \mathbf{1}n_A + \bar{\mathbf{J}}_{CB}^T \cdot \mathbf{1}n_B \\ \bar{w}_{T,A} &= \bar{\mathbf{J}}_{CA}^T \cdot \mathbf{1}t_A + \bar{\mathbf{J}}_{CB}^T \cdot \mathbf{1}t_B \end{aligned} \quad (32)$$

The scalars \bar{w}_N and \bar{w}_T were not mentioned before and are needed when solving the contact problems [17].

3.2 Collision detection

It would be very time-consuming to check each point whether it is penetrating into another body. It is a common practice, therefore, to build bounding objects that are geometrically simple and can be used for fast overlapping checks. Very often bounding boxes (BB) and bounding spheres are used. As this is quite an inaccurate method of collision detection, more advanced methods have been developed, e.g. polygon bounding objects, BB tree hierarchies and so on [24, 25].

The accuracy of bounding-objects methods depends on the BB size, which for our application is still not accurately enough. Because a fast and exact collision detection is needed, a two-stage method for collision detection is used. The first step is collision detection on object-oriented BB (OOBB) trees and the second step is exact collision detection on the point-to-point level.

3.2.1 BB tree overlapping

Before the simulation starts for each body, an axis-aligned (in the body coordinate system) BB tree

(AABB) is created. The main BB includes the whole body; in the next level, two children BBs are created (each containing half of the points of the parent). The process of creating a child BB is repeated until there exists a BB with more than the minimum number of points (i.e. two or three) (Fig. 7).

When such an AABB is rotated we use it as an OOBB. When a collision detection between two bodies is made, the top BBs are checked first. If overlapping exists, then the children are checked. This overlapping check is repeated until there are children BBs.

3.2.2 Exact collision detection

When two BBs without children overlap, then a check for a possible exact point of penetration needs to be done (Fig. 8). We have to check whether body A is penetrating into body B and also vice versa. If point C (body B) penetrates the border AB of the penetrating body (body A) then the following tests are positive (Fig. 9)

$$\mathbf{AB} \times \mathbf{AC} \geq 0 \quad \text{C is on the left of AB} \quad (33)$$

$$\angle BAC \leq \frac{\varphi_A}{2} \quad \text{angle at A} \quad (34)$$

$$\angle ABC \leq \frac{\varphi_B}{2} \quad \text{angle at B} \quad (35)$$

$$|h| < s \quad \text{maximum depth} \quad (36)$$

where

$$\mathbf{AB} = \mathbf{r}_B - \mathbf{r}_A, \quad \mathbf{AC} = \mathbf{r}_C - \mathbf{r}_A \quad (37)$$

The distance h is depicted in Fig. 9; s is a parameter that needs to be set and should be several times (10–100 times) greater than the maximum-allowed penetration depth. After collision detection, a parameter s is used to identify whether the time-step is too large, i.e. if h is greater than the maximum-allowed penetration depth, but a collision is identified, then it is clear that the change of the positions of the bodies is too large. If instead of s the maximum penetration depth was to be used, then in such a case mistakenly no collision would be identified.

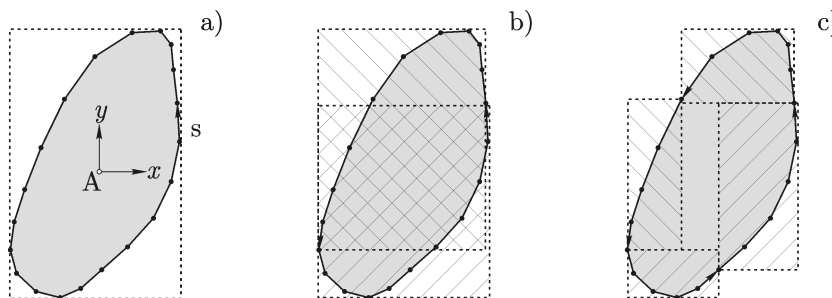


Fig. 7 Hierarchy of AABB tree: (a) first level, (b) second level, and (c) third level

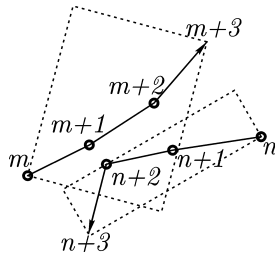


Fig. 8 Overlapping BBs without children

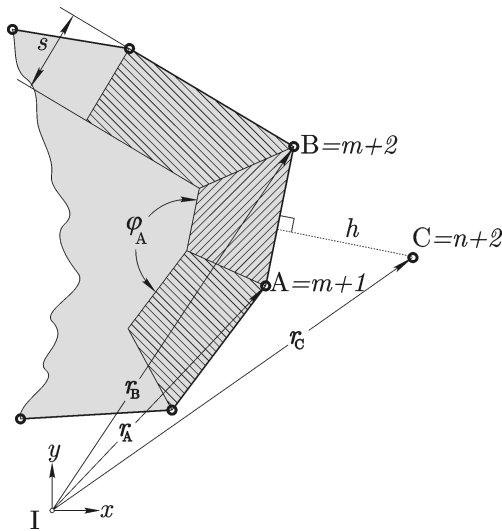


Fig. 9 Penetrated body (shaded) and possibly penetrating point C. Hatched region shows the 'skin' of the penetrated body

4 NUMERICAL EXAMPLES

The woodpecker toy is a good example of a system with multiple impacts and stick–slip phenomena. In this investigation, the woodpecker toy is studied as a three-degrees-of-freedom (3-DOF) system and also as a four-degrees-of-freedom (4-DOF) system. The results are compared with the previous studies of the woodpecker toy: Glocker [18] and Leine *et al.* [19]. The 3-DOF model was experimentally verified by Pfeiffer and [17].

A mechanical model of the woodpecker toy is shown in Fig. 10.

1. Dynamics. $m_M = 0.0003$ kg, $J_M = 5.0 \times 10^{-9}$ kg m², $m_S = 0.0045$ kg, $J_S = 7.0 \times 10^{-7}$ kg m², $g = 9.81$ m s⁻², and $c_\varphi = 0.0056$ Nm/rad.
2. Geometry. $r_0 = 0.0025$ m, $r_M = 0.0031$ m, $h_M = 0.0058$ m, $l_M = 0.010$ m, $l_G = 0.015$ m, $h_S = 0.020$ m, $l_S = 0.0201$ m, and $r_S = 0.002$ m.
3. Contact. sleeve-pole: $\mu = 0.3$, $\epsilon_N = 0$, $\epsilon_T = 0$, and $\nu = 0$, sleeve-woodpecker: $\mu = 0.3$, $\epsilon_N = 0.5$, $\epsilon_T = 0$, and $\nu = 0$.

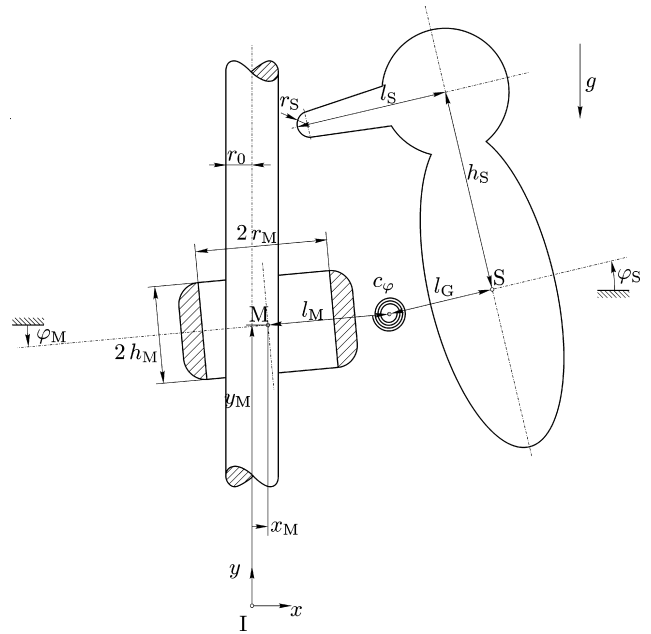


Fig. 10 Mechanical model (not to scale)

4.1 3-DOF model with small-angle approximation

The set of generalized coordinates is

$$q = \begin{pmatrix} y_M \\ \varphi_M \\ \varphi_S \end{pmatrix} \tag{38}$$

The coordinate $x_M = 0$ is constant. The approximation of small angles is taken into account: $\sin \varphi \approx \varphi$, $\cos \varphi \approx 1$.

The mass matrix M and the force vector h are

$$M = \begin{pmatrix} m_M + m_S & l_M m_S & l_G m_S \\ l_M m_S & J_M + l_M^2 m_S & l_G l_M m_S \\ l_G m_S & l_G l_M m_S & J_S + l_G^2 m_S \end{pmatrix} \tag{39}$$

$$h = \begin{pmatrix} -g(m_S + m_M) \\ -gl_M m_S + c_\varphi \varphi_S - c_\varphi \varphi_M \\ -gl_G m_S - c_\varphi \varphi_S + c_\varphi \varphi_M \end{pmatrix} \tag{40}$$

The contact points and the appropriate kinematic properties included in W_N , W_T , \bar{w}_N , and \bar{w}_T are automatically generated during a collision from the geometry of the bodies and their kinematics. However, in the 3-DOF model, the exact contact points are known in advance, as are their kinematical properties [17, 19].

The contact of the beak of the woodpecker with the pole is characterized by

$$\bar{w}_{N,1} = \begin{pmatrix} 0 \\ 0 \\ -h_S \end{pmatrix} \quad \bar{w}_{T,1} = \begin{pmatrix} 1 \\ l_M \\ l_G - l_S \end{pmatrix} \tag{41}$$

In addition, the contacts of the lower edge and the upper edge of the sleeve with the pole are characterized by

$$\bar{w}_{N,2} = \begin{pmatrix} 0 \\ h_M \\ 0 \end{pmatrix} \quad \bar{w}_{T,2} = \begin{pmatrix} 1 \\ r_M \\ 0 \end{pmatrix} \quad (42)$$

$$\bar{w}_{N,3} = \begin{pmatrix} 0 \\ -h_M \\ 0 \end{pmatrix} \quad \bar{w}_{T,3} = \begin{pmatrix} 1 \\ r_M \\ 0 \end{pmatrix} \quad (43)$$

The remaining vectors are $\bar{w}_N = 0$ and $\bar{w}_T = 0$. The results are given in Fig. 11.

4.2 4-DOF model

The set of generalized coordinates is

$$q = \begin{pmatrix} x_M \\ y_M \\ \varphi_M \\ \varphi_S \end{pmatrix} \quad (44)$$

The mass matrix \mathbf{M} and the force vector \mathbf{h} are

$$\mathbf{M} = \begin{pmatrix} m_S + m_M & 0 & -l_M m_S \sin \varphi_M & \dots \\ & m_S + m_M & l_M m_S \cos \varphi_M & \dots \\ & & J_M + l_M^2 m_S (\cos \varphi_M)^2 & \dots \\ & & & + l_M^2 m_S (\sin \varphi_M)^2 \\ \text{symmetric} & & & \\ & & -l_G m_S \sin \varphi_S & \\ & & l_G m_S \cos \varphi_S & \\ & & l_G l_M m_S \cos \varphi_S \cos \varphi_M + l_G l_M m_S \sin \varphi_S \sin \varphi_M & \\ & & & J_S + l_G^2 m_S (\cos \varphi_S)^2 + l_G^2 m_S (\sin \varphi_S)^2 \end{pmatrix} \quad (45)$$

$$\mathbf{h} = \begin{pmatrix} m_S (l_G \dot{\varphi}_S^2 \cos \varphi_S + l_M \dot{\varphi}_M^2) \cos \varphi_M \\ -g(m_S + m_M) + l_G m_S \dot{\varphi}_S^2 \sin \varphi_S + l_M m_S \dot{\varphi}_M^2 \sin \varphi_M \\ c_\varphi \varphi_S - c_\varphi \varphi_M + l_M m_S (-g \cos \varphi_M + l_G \dot{\varphi}_S^2 \sin(\varphi_S - \varphi_M)) \\ -c_\varphi \varphi_S + c_\varphi \varphi_M - l_G m_S \dot{\varphi}_M^2 (g \cos \varphi_S + l_M \sin(\varphi_S - \varphi_M)) \end{pmatrix} \quad (46)$$

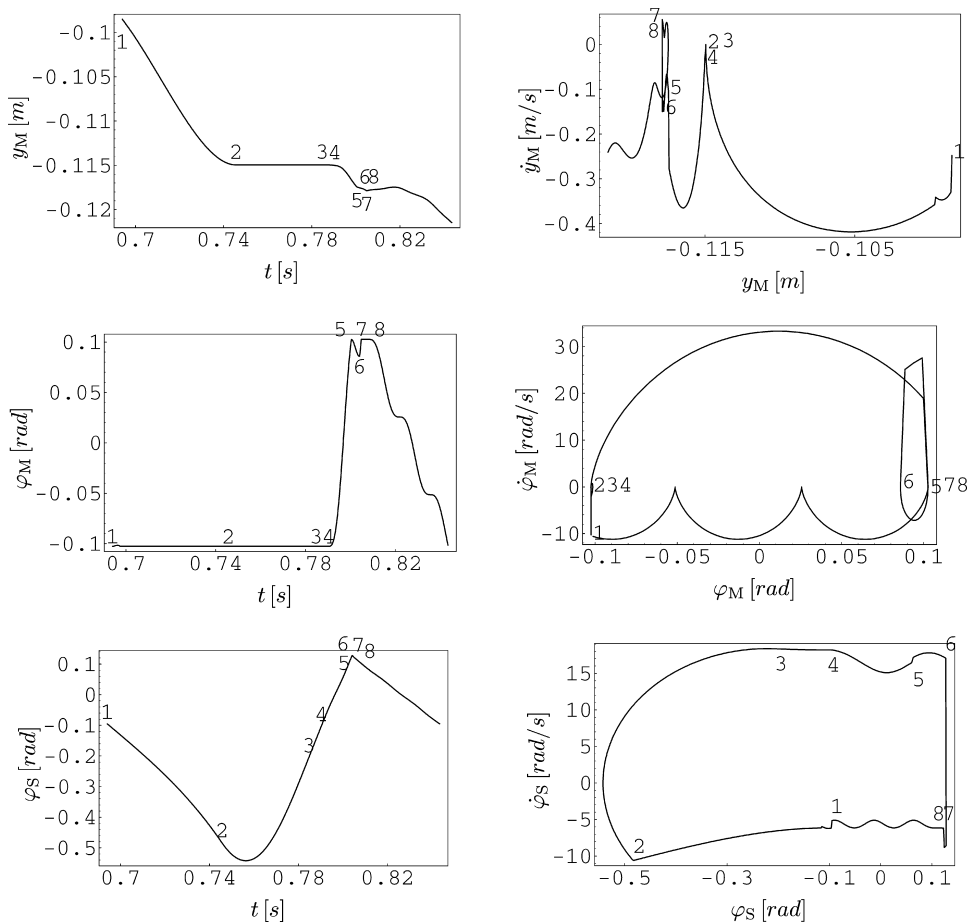


Fig. 11 Results of the 3-DOF model. Left: in time domain, right: phase-space portraits

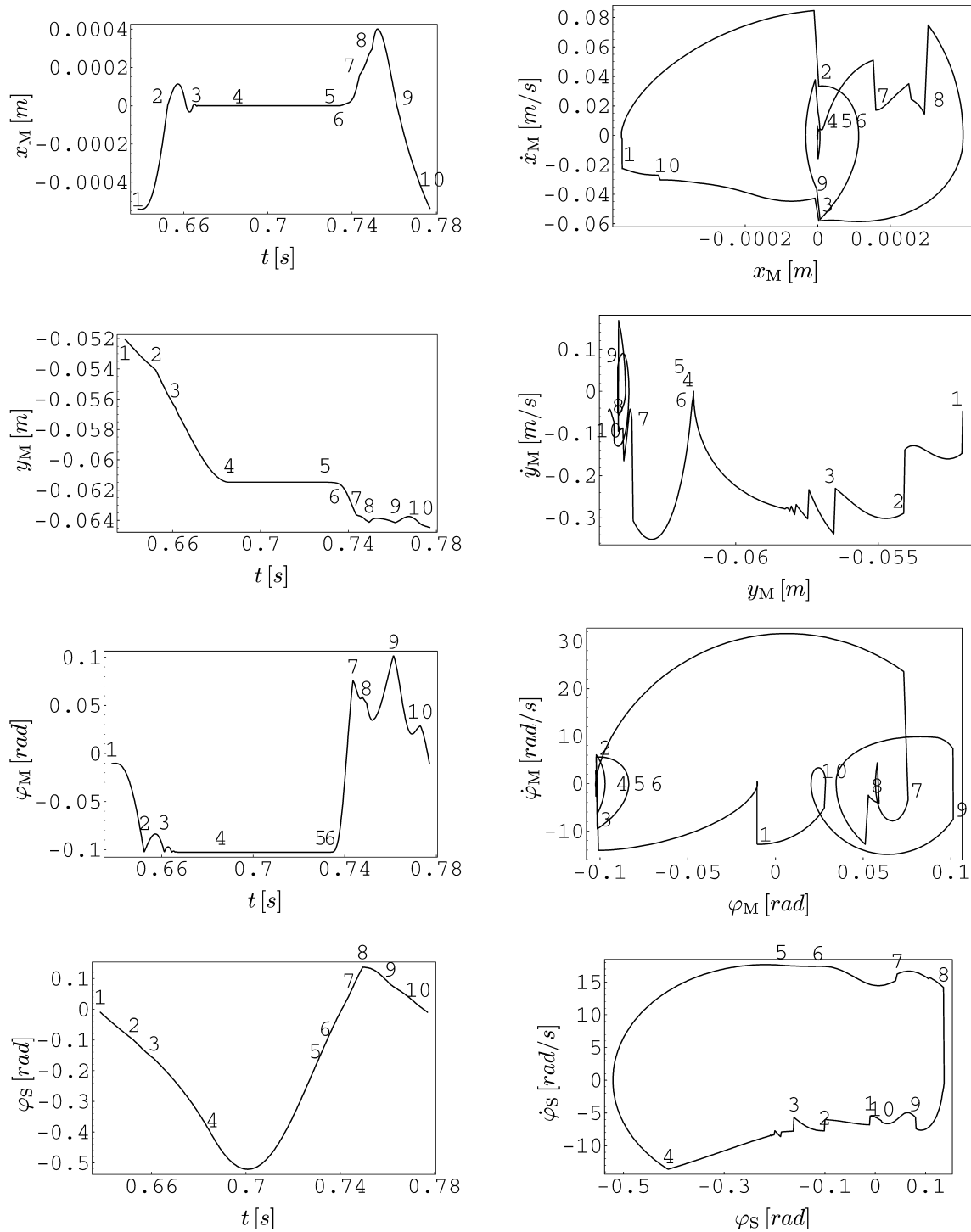


Fig. 12 Results of 4-DOF model. Left: in time domain, right: phase-space portraits

In this case, the actual contact point of the beak and the pole is not known and the kinematical properties of the contact points \mathbf{W}_N , \mathbf{W}_T , $\bar{\mathbf{w}}_N$, and $\bar{\mathbf{w}}_T$ are non-linearly dependent on generalized coordinates and need to be recalculated during each step according to equations (31) and (32). The results are given in Fig. 12.

4.3 Comparison and verification of the 3- and 4-DOF models

In Table 1, the more important events of the 3- and 4-DOF models are described. Whereas previous work on the woodpecker toy was based on a 3-DOF mechanical model with a small-angle approximation

Table 1 Comparison of key events for the 3- and 4-DOF models

3-DOF model			4-DOF model		
No.	Description	t (ms)	No.	Description	t (ms)
1	Impact of sleeve then slipping of sleeve	0.0	1	Impact of sleeve (LR)	0.0
2	Slip-stick transition of sleeve	51.4	2	Impact of sleeve (UL), detachment of sleeve (LR)	14.2
3	Stick-slip transition of sleeve	90.6	3	Impact of sleeve (LR)	22.8
4	Detachment of sleeve	96.2	4	Slip-stick transition of sleeve	47.4
5	Impact then slipping of sleeve	106.4	5	Stick-slip transition of sleeve	91.2
6	Impact (woodpecker beak)	110.0	6	Detachment of sleeve (LR and UL)	95.4
7	Impact of sleeve	110.8	7	Impact (LL) then slipping of sleeve	105.4
8	Detachment of sleeve	114.0	8	Impact (woodpecker beak)	111.2
1	Impact of sleeve then slipping of sleeve	149.4	9	Detachment of sleeve (LR and UL)	123.2
			10	Impact of sleeve (UR) then detachment	134.8
			1	Impact of sleeve (LR)	138.8

L, lower; U, upper; R, right; and L, left.

[17–19], this study presents the mechanical model with 4-DOF and without the small-angle approximation.

By comparing the 3-DOF model presented in this investigation with the study of Leine *et al.* [19], we see that the results are in close accordance. The period of the solution is $T \approx 0.15$ s, the vertical displacement is $\Delta y_M \approx 23$ mm, and the phase-space portraits are practically the same.

However, the influence on the dynamics of the wooden toy of the additional degree of freedom x_M and the non-linear mass matrix \mathbf{M} and the non-linear vector \mathbf{h} showed up as quite important. The biggest difference between the 3- and 4-DOF models can be seen in the vertical displacement of the sleeve, which is much smaller in the case of the 4-DOF model: $\Delta y_M = 12$ mm (Fig. 13). Consequentially, the period decreased to $T \approx 0.14$ s. The phase-space portraits of the coordinates φ_M , φ_S are, however, qualitatively comparable.

Glocker [18] experimentally measured the vertical displacement of the woodpecker to be $\Delta y_M \approx 5.3$ mm. As the 3- and 4-DOF models differ

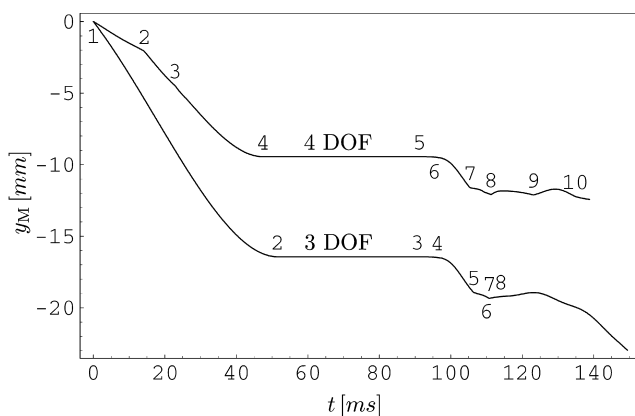


Fig. 13 Relative displacement in the vertical direction of the 3- and 4-DOF model

mainly in the vertical displacement and as the 4-DOF is closer to the experimental displacement, we can assume that the details added to the 4-DOF model help to build an adequate dynamical model.

5 CONCLUSIONS

This article presents the use of the Pfeiffer–Glocker [17] formulation of multi-body dynamics with unilateral contacts on discretely defined bodies. The mathematical notation of stick–slip or detachment including impacts with friction and the reversibility in the tangential direction was adopted to

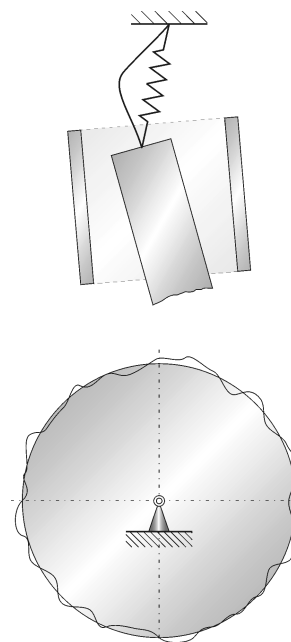


Fig. 14 Electric-brush dynamics: sliding, sticking, and impacting against rough commutator-surface and brush-guidance

discretely defined bodies. In discrete bodies, the number of possible contact points cannot be foreseen, and therefore it is necessary that the contact-points sets and the necessary contact kinematics are created during runtime.

The Pfeiffer–Glocker formulation proved to be useful in several applications on gear rattling, turbine blade dampers, friction clutch vibrations, drilling machine, and soon [17]. This formulation can now be expanded towards rigid bodies with body-shapes which cannot be determined by simple mathematical functions, i.e. electric-brush dynamics with rough contact surfaces see (Fig. 14).

The exact collision detection of discrete bodies is a bottleneck in numerical simulations. The presented two-step collision detection combines the speed of BB trees and the precision of vector analysis.

To show the benefits of the presented procedures, a numerical example of the woodpecker toy with geometrical non-linearities and concurrent stick-slip and impact events is compared with previous studies. It revealed that the additional degree of freedom and non-linearities introduced by the 4-DOF model produce qualitatively and partly quantitatively comparable results with the 3-DOF model.

However, the vertical displacement of the woodpecker differs from previous models for ~50 per cent. The reason for the difference in the vertical displacement is the additional horizontal degree of freedom introduced by the 4-DOF model, which changes the mechanism of the jamming of the sleeve. The presented 4-DOF model is assumed to be more realistic.

REFERENCES

- 1 **Vereshchagin, A. F.** Computer simulation of the dynamics of complicated mechanisms of robot manipulations. *Eng. Cybern.*, 1974, **6**, 65–70.
- 2 **Armstrong, W. W.** and **Green, M. W.** The dynamics of articulated rigid bodies for purposes of animation. *Visual Comput.*, 1985, **1**, 231–240.
- 3 **Featherstone, R.** *Robot dynamics algorithms*, 1987 (Kluwer, Norwell, MA).
- 4 **Lötstedt, P.** Coulomb friction in two-dimensional rigid body systems. *Z. Angewandte Math. Mech.*, 1981, **61**, 605–615.
- 5 **Lötstedt, P.** Mechanical systems of rigid bodies subject to unilateral constraints. *SIAM J. Appl. Math.*, 1982, **42**(2), 281–296.
- 6 **Murty, K. G.** *Linear complementarity, linear and non-linear programming*, 1988 (Heldermann Verlag, Berlin), available from http://ioe.engin.umich.edu/people/fac/books/murty/linear_complementarity_webbook/.
- 7 **Baraff, D.** *Dynamic simulations of non-penetrating rigid bodies*. PhD Thesis, Cornell University, NY, 1992.
- 8 **Panagiotopoulos, P. D.** *Hemivariational inequalities: applications in mechanics and engineering*, 1993 (Springer Verlag, Berlin, Heidelberg).
- 9 **Moreau, J. J.** Sur les mesures différentielles de fonctions vectorielles et certain problèmes d'évolution. *Comptes Rendus Acad. Sci. Paris*, 1976, **282**, 837–840.
- 10 **Mirtich, M.** and **Canny, J. F.** Impulse-based simulation of rigid bodies. In Proceedings of Symposium on Interactive 3D Graphics, ACM SIGGRAPH, 1995, Vol. 217, pp. 181–188.
- 11 **Moreau, J. J.** Formulation of contact with dry friction – computational application. *Comptes Rendus de l' Acad. Sci. Serie II*, 1998, **302**(13), 799–801.
- 12 **Mirtich, B.** and **Canny, J.** Impulse-based dynamic simulation. In *The algorithmic foundations of robotics* (Eds K. Golberg, D. Halperin, J. C. Latombe, and R. Wilson) 1994 (A.K. Peters, Boston).
- 13 **Monteiro-Marques, M. D. P.** *Differential inclusions in nonsmooth mechanical problems: shocks and dry friction*, 1993, Vol. 9 (Birkhäuser Verlag, Basel, Boston, Berlin).
- 14 **Stewart, D. E.** and **Trinkle, J. C.** An implicit time-stepping scheme for rigid body dynamics with inelastic collisions and coulomb friction. *J. Num. Methods Eng.*, 1996, **39**, 2673–2691.
- 15 **Stewart, D. E.** Rigid-body dynamics with friction and impact. *SIAM Rev.*, 2000, **42**(1), 39.
- 16 **Anitescu, M.** and **Potra, F. A.** Formulating dynamic multi-rigidbody contact problems with friction as solvable linear complementarity problems. *Nonlinear Dynam.*, 1997, **14**, 231–247.
- 17 **Pfeiffer, F.** and **Glocker, C.** *Multi-body dynamics with unilateral contacts*, 1996 (John Wiley & Sons, Inc., New York)
- 18 **Glocker, C.** *Dynamik von Starrkörpersystemen mit Reibung und Stößen*. PhD Thesis, Technische Universität München, 1995.
- 19 **Leine, R. I., Glocker, C.,** and **Van Campen, D. H.** Non-linear dynamics and modelling of some wooden toys with impact and friction. *J. Vib. Control*, 2003, **9**, 25–78.
- 20 **Pfeiffer, F.** The idea of complementarity in multi-body dynamics. *Arch. Appl. Mech.*, 2003, **72**, 807–816.
- 21 **Cottle, R. W.** and **Dantzig, G. B.** Complementary pivot theory of mathematical programming. *Linear Algebra Appl.*, 1968, **1**, 103–125.
- 22 **Cline, M. B.** *Rigid body simulation with contact and constraints*. Master's Thesis, The University of British Columbia, 1999.
- 23 **Golub, G. H.** and **Loan, C. F.** *Matrix computations*. 3rd edition, 1996 (Johns Hopkins Univ. Press).
- 24 **Klosowaski, J. T.** *Efficient collision detection for interactive 3D graphics and virtual environments*. PhD Thesis, Applied Mathematics and Statistics, State University of New York at Stony Brook, 1998.
- 25 **Zachmann, G.** *Virtual reality in assembly simulation – collision detection, simulation algorithms, and interaction techniques*. PhD Thesis, Technische Universität Darmstadt, 2000.

APPENDIX

Notation

- | | |
|----------------------|---|
| A | known matrix in LCP |
| A_A | transformation matrix from the relative frame A to the inertial frame I |

\mathbf{b}	known vector in LCP	\mathbf{W}_N	matrix of kinematical properties in normal direction of a set of contact points
f	degrees of freedom	\mathbf{W}_T	matrix of kinematical properties in tangential direction of a set of contact points
$\mathbf{F}_{A,N}$	vector of normal contact force at point C_A on the body A	\mathbf{w}_N	vector of kinematical properties in normal direction of a contact point
$\mathbf{F}_{A,T}$	vector of tangential contact force at point C_A on the body A	\mathbf{w}_T	vector of kinematical properties in tangential direction of a contact point
\mathbf{g}_N	vector of relative contact coordinates in normal direction	\mathbf{x}	unknown vector in LCP
\mathbf{g}_T	vector of relative contact coordinates in tangential direction	\mathbf{y}	unknown vector in LCP
\mathbf{h}	vector of generalized active forces	φ_A	rotational degree of freedom for body A
\mathbf{j}_A	vector of acceleration parameters of the centre of gravity of A which do not depend on the generalized accelerations	λ_N	amplitude of contact force in normal direction
\mathbf{J}_A	Jacobian matrix because of translation of centre of gravity	λ_T	amplitude of contact force in tangential direction
$\mathbf{J}_{C_A}^T$	the Jacobian matrix of ${}^i\mathbf{r}_{C_A}$	$\boldsymbol{\lambda}_N$	vector of amplitudes of contact forces in normal direction
$\mathbf{J}_{C_B}^T$	the Jacobian matrix of ${}^i\mathbf{r}_{C_B}$	$\boldsymbol{\lambda}_T$	vector of amplitudes of contact forces in tangential direction
\mathbf{J}_{RA}	Jacobian matrix because of rotation of centre of gravity	$\boldsymbol{\Lambda}_{NC}$	vector of contact impulses (normal) in compression phase
\mathbf{M}	mass matrix	$\boldsymbol{\Lambda}_{TC}$	vector of contact impulses (tangential) in compression phase
${}^i\mathbf{n}_A$	normal vector at contact point	$\boldsymbol{\Lambda}_{NE}$	vector of contact impulses (normal) in expansion phase
\mathbf{q}	vector of generalized coordinates	$\boldsymbol{\Lambda}_{TE}$	vector of contact impulses (tangential) in expansion phase
\mathbf{Q}_i^C	vector of generalized, non-conservative active forces	$\bar{\boldsymbol{\mu}}$	diagonal matrix of friction coefficients
${}^i\mathbf{r}_{C_A}$	vector to point C_A on the body A		
t_A	start time of compression phase		
${}^i\mathbf{t}_A$	tangent vector at contact point		
t_C	end time of compression phase and start time of expansion phase		
t_E	end time of expansion phase		